$V^{III}V^{IV}{}_3O_3(PO_4)_3$: A Novel Vanadium Phosphate for Selective Oxidation of Light Hydrocarbons

Ernst Benser,[†] Robert Glaum,*[,†] Thomas Dross,[†] and Hartmut Hibst[‡]

Institut für Anorganische Chemie, Universität Bonn, Gerhard-Domagk-Strasse 1, D-53121 Bonn, Germany, and BASF AG, Carl-Bosch-Strasse 38, D-67056 Ludwigshafen, Germany

Received April 16, 2007. Revised Manuscript Received June 15, 2007

A novel vanadium(IV) phosphate $V^{III}V^{IV}{}_3O_3(PO_4)_3$ has been synthesized and crystallized (1073 K, sealed silica tube, a few milligrams of $PtCl_2$ as mineralizer). According to the single-crystal structure analysis [orthorhombic, *F*2*dd* (No. 63), $Z = 24$, $a = 7.2596(8)$ Å, $b = 21.786(2)$ Å, $c = 38.904(4)$ Å (lattice parameters from Guinier photographs), $R_1 = 0.032$, $wR_2 = 0.067$, κ-CCD diffractometer, 83 949 reflections measured, 6836 independent, 5986 with $I > 2\sigma(I)$, 299 variables], $V^{III}V^{IV}{}_3O_3(PO_4)_3$ belongs to the Lipscombite/Lazulite structure family. At 1073 K $V^{III}V^{IV}{}_3O_3(PO_4)_3$ is in thermodynamic equilibrium with $(VO)_2P_2O_7$, VO_2, and VPO_4. Substitution of V^{3+} in $V^{III}V^{IV}{}_3O_3(PO_4)_3$ by Cr^{3+} and Fe^{3+} is possible. Like vanadylpyrophosphate the oxide phosphates $M^{III}V^{IV}{}_3O_3(PO_4)_3$ (M^{III}: V, Cr, Fe) show significant catalytic activity in selective oxidation of *n*-butane and 1-butene to maleic acid anhydride.

Introduction

Vanadylpyrophoshate is used as a heterogeneous catalyst for the industrial oxidation of *n*-butane to maleic acid anhydride (MA) as well as in several other oxidation reactions.[1,2] Therefore, it has been the subject of numerous investigations during the past 30 years. It is often reported that modification ("tuning") of $(VO)_2P_2O_7$ with (transition) metal oxides leads to a promoting effect on the catalytic activity of $(VO)_2P_2O_7$.[3,4] Whether such effects are due to crystal chemical inclusion of the promoting oxide into the $(VO)_2P_2O_7$ lattice (formation of solid solutions), to formation of new polynary phosphate phases, or simply to kinetic effects on the crystallization of vanadylpyrophosphate remains widely in the dark.

It is rather surprising that, despite the tremendous economical importance and the great scientific interest in $(VO)_2P_2O_7$, up to now no systematic investigation on the solid phases and their relationship in the ternary system V/P/O has been published. We have established in recent years only the phase relations for this system (Figure 1).[5−7] Under equilibrium conditions at 1073 K, 10 phosphates are existing in the ternary system vanadium/phosphorus/oxygen.[5−7] This rather high number of vanadium phosphates, only surpassed by the number of iron phosphates,[6,8] is due to the ability of vanadium to form various oxidation states and to the stability of phosphates with a wide range of ratios *n*(vanadium oxide)/*n*(phosphorus oxide). A survey of chemically and structurally characterized anhydrous vanadium phosphates is given in Table 1.

The first mixed-valence vanadium(III,IV) phosphate to be discovered was $V_2(VO)(P_2O_7)_2$.[15] In literature a compound "$V_3P_2O_{11}$" (described as oxide diphosphate "$V_3O_4(P_2O_7)$") is mentioned; however, no further evidence is provided by the authors.[23] An interesting phosphate is $V_2(PO_4)_3$ with vanadium(IV,V). This nasicon type phosphate can only be obtained by oxidative electrochemical deintercalation of $Na_3V_2(PO_4)_3$.[20] It does not exist at 1073 K as a thermodynamically stable equilibrium phase.

[†] Universität Bonn.
[‡] BASF AG.

(1) Ebner, J.; Thompson, M. *Studies in Surface Science and Catalysis*; Elsevier: New York, 1992.
(2) Hodnett, K. *Heterogenous Catalytic Oxidation*; John Wiley & Sons: Chichester, 2000.
(3) Narayana, K. V.; Martin, A.; Lücke, B.; Belmans, M.; Boers, F.; Van Deynse, D. *Z. Anorg. Allg. Chem.* **2005**, *631*, 25−30.
(4) Hutchings, G. J.; Higgins, R. *J. Catal.* **1996**, *162*, 153.
(5) Kaiser, U. Ph.D. Thesis, University of Giessen, 1996.
(6) Glaum, R. Neue Untersuchungen an wasserfreien Phosphaten der Übergangsmetalle (in German). Thesis of Habilitation, University of Giessen, 1999 (URL: http://bibd.uni-giessen.de/ghtm/1999/uni/h990001.htm).
(7) Dross, T. Ph.D. Thesis, University of Bonn, 2002. (URL: http://hss.ulb.uni-bonn.de/diss_online/math_nat_fak/2004/dross_thomas/index.htm).
(8) Gleitzer, C. *Eur. J. Inorg. Solid State Chem.* **1991**, *28*, 77−91.
(9) Glaum, R.; Gruehn, R. *Z. Kristallogr.* **1989**, *186*, 91−93.
(10) Modaressi, A.; Courtois, A.; Gerardin, R.; Malaman, B.; Gleitzer, C. *J. Solid State Chem.* **1981**, *40*, 301−311.
(11) Glaum, R.; Gruehn, R. *Z. Kristallogr.* **1992**, *198*, 41−47.
(12) Palkina, K. K.; Maksimova, S. I.; Chibiskova, N. T.; Schlesinger, K.; Ladwig, G. *Z. Anorg. Allg. Chem.* **1985**, *529*, 89−96.
(13) Lii, K.-H.; Chen, Y. B.; Su, C. C.; Wang, S.-L. *J. Solid State Chem.* **1989**, *82*, 156−160.
(14) Middlemiss, N.; Hawthorne, F. C.; Calvo, C. *Can. J. Chem.* **1977**, *55*, 1673−1679.
(15) Johnson, J. W.; Johnston, D. C.; King, H. R., Jr.; Halbert, T. R.; Brody, J. F.; Goshorn, D. P. *Inorg. Chem.* **1988**, *27*, 1646−1648.
(16) Gorbunova, Yu. E.; Linde, S. A. *Dokl. Akad. Nauk SSSR* **1979**, *245*, 584−588.
(17) Geupel, S.; Pilz, K.; van Smaalen, S.; Buellesfeld, F.; Prokofiev, A.; Assmus, W. *Acta Crystallogr.* **2002**, *C58*, 9−13.
(18) Murashova, E. V.; Chudinova, N. N. *Kristallografiya* **1994**, *39*, 145−146.
(19) Krasnikov, V. V.; Konstant, Z. A. *Izv. Akad. Nauk SSSR, Neorg. Mater.* **1979**, *15*, 2164−2167.
(20) Gopalakrishnan, J.; Rangan, K. K. *Chem. Mater.* **1992**, *4*, 745−747.
(21) Jordan, B.; Calvo, C. *Can. J. Chem.* **1973**, *51*, 2621−2625.
(22) Gopal, R.; Calvo, C. *J. Solid State Chem.* **1972**, *5*, 432−435.
(23) Golovkin, B. G.; Volkov, V. L. *Russ. J. Inorg. Chem.* **1987**, *32*, 739−741.

10.1021/cm071036u CCC: $37.00
Published on Web 07/21/2007

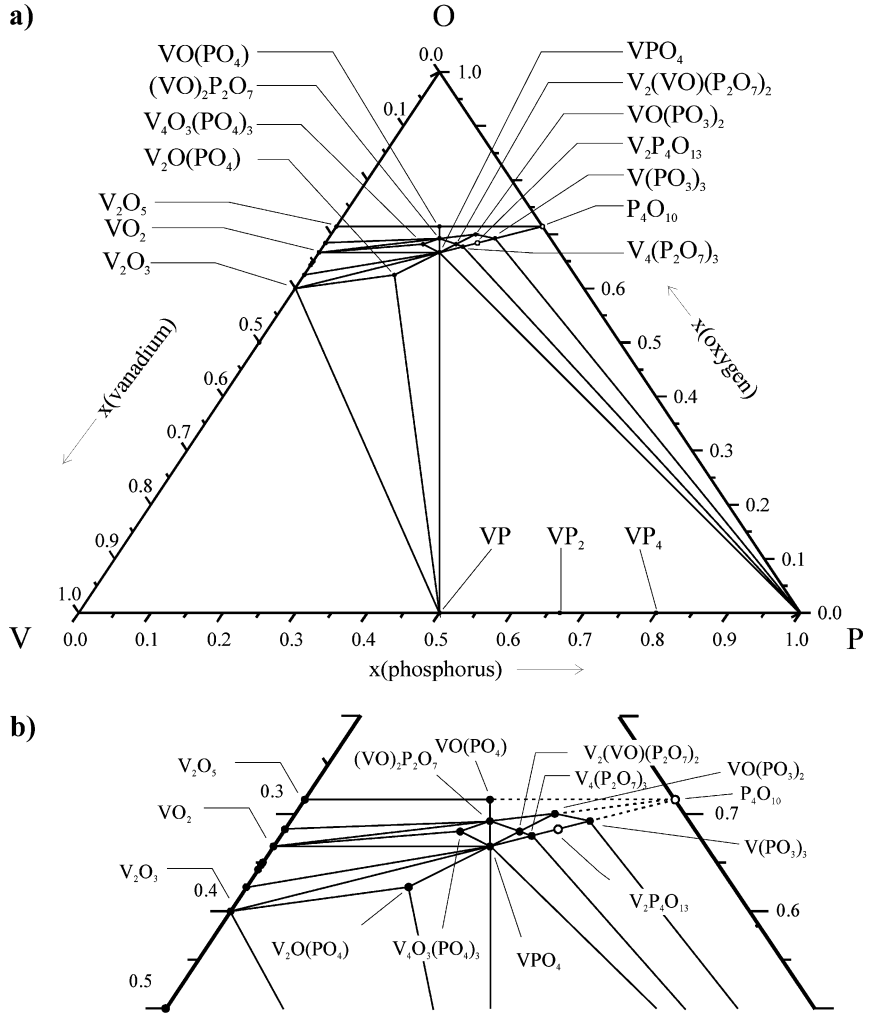

Figure 1. Ternary phase diagram V/P/O at 1173 K (a). Section of the phase triangle showing all anhydrous vanadium phosphates (b). $V_2P_4O_{13}$ is metastable to decomposition into $V_4(P_2O_7)_3$ and $V(PO_3)_3$. VP_2 and VP_4 exist only under higher phosphorus equilibrium pressures. The section V/VP/VO has not been investigated yet.

Table 1. Chemically and Structurally Characterized Anhydrous Vanadium Phosphates

oxidation state	phosphate
II+/III+	α-/β-$V_2O(PO_4)$[a,9]
III+	VPO_4,[11] $V_4(P_2O_7)_3$,[12] $V_2P_4O_{13}$,[b,5,7] $V(PO_3)_3$[13]
III+/IV+	$\square_2V_4O_3(PO_4)_3$,[c] $V_2(VO)(P_2O_7)_2$[15]
IV+	$(VO)_2P_2O_7$,[16,17] $VO(PO_3)_2$[18,19]
IV+/V+	$V_2(PO_4)_3$[20,d]
V+	$\alpha_{I,II}$-/β-/γ-/δ-$VOPO_4$[21,22]

[a] $V_2O(PO_4)$ is isotypic to β-$Fe_2O(PO_4)$,[10] the aristotype of the Lipscombite/Lazulite structure family. [b] Vanadium(III) tetraphosphate is isotypic to $Cr_2P_4O_{13}$[13] and apparently thermodynamically metastable toward decomposition into $V_4(P_2O_7)_3$ and $V(PO_3)_3$. [c] This paper. [d] Vanadium(IV,V) phosphate with nasicon structure has been synthesized by topotactic, oxidative deintercalation of $Na_3V_2(PO_4)_3$ at rather low temperatures. The decomposition temperature is not given in the reference, but it is mentioned that synthesis of $V_2(PO_4)_3$ at high temperatures by solid-state reaction is not possible.[20]

Equilibrium experiments in the region $(VO)_2P_2O_7/VPO_4/VO_2$ of the V/P/O system provided the first evidence for a hitherto unknown vanadium phosphate.[7] The X-ray powder diffraction pattern of the new phase showed strong resemblance to that of the mixed-valence titanium(III,IV) oxide phosphate $Ti_4O_3(PO_4)_3$.[24−26] In the present paper we report on synthesis, crystallization, crystal structure, and catalytic behavior of the new vanadium(III,IV) oxide phosphate. It was of particular interest to our study to investigate the substitution of vanadium in $V_4O_3(PO_4)_3$ by other metals and to characterize the redox behavior of the oxide phosphate, the latter attribute being the key to understanding of the catalytic activity of vanadium phosphates[27] in selective oxidation reactions of alkanes.

Experimental Section

Starting Materials. Starting materials for the experiments were synthesized according to literature procedures. V_2O_3 was obtained reducing V_2O_5 by H_2 at 1073 K.[28] VO_2 was synthesized by symproportionation of 1 mmol V_2O_5 (MERCK) with 1 mmol of V_2O_3 (sealed silica ampule, isothermal heating at $T = 1073$ K, addition of 80 mg of iodine as mineralizer).[29] VPO_4[11] was synthesized from VP[30] and β-$VOPO_4$.[22] It was subsequently

(24) Reinauer, F.; Glaum, R.; Gruehn, R. *Eur. J. Solid State Inorg. Chem.* **1994**, *31*, 779−791.
(25) Reinauer, F.; Glaum, R. *Acta Crystallogr.* **1998**, *B54*, 722−731.
(26) Schöneborn, M.; Glaum, R. *J. Solid State Chem.* **2007**, in preparation.
(27) Patent pending.
(28) Oppermann, H.; Reichelt, W.; Krabbes, G.; Wolf, E. *Z. Anorg. Allg. Chem.* **1977**, *432*, 26−32.
(29) Oppermann, H.; Reichelt, W.; Krabbes, G.; Wolf, E. *Krist. Tech.* **1977**, *12*, 717−728.
(30) Glaum, R.; Gruehn, R. *Z. Anorg. Allg. Chem.* **1989**, *568*, 73−84.

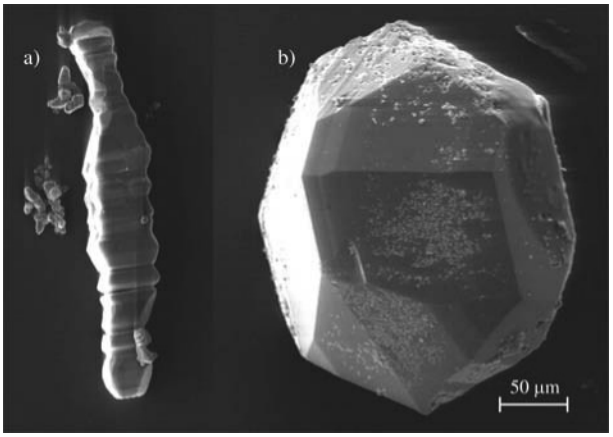

Figure 2. Scanning electron micrographs showing typical crystal shapes of $V_4O_3(PO_4)_3$. Pillar of several intergrown crystals (a) and single crystal used for diffraction measurement (b).

crystallized by chemical vapor transport.[31,32] $(VO)_2P_2O_7$ was obtained by heating $VO(HPO_4)\cdot(1/2)H_2O$ in flowing argon at 1073 K.[33] Vanadyl-hydrogenphosphate-hemihydrate was synthesized by the "organic route", refluxing V_2O_5 and H_3PO_4 (MERCK) in *n*-butanole.[33]

Synthesis and Crystallization of $V_4O_3(PO_4)_3$. According to reaction 1, vanadium(III,IV) oxide phosphate was obtained from 0.77 mmol of VO_2, 0.77 mmol of VPO_4, and 0.77 mmol of $(VO)_2P_2O_7$. The educts were ground and mixed together in an agate mortar, pressed into a tablet, and soaked for 5 days at 1073 K in a sealed silica tube. A corundum crucible within the ampule prevented the reaction with the silica wall. From differential thermal analysis experiments, $mp(V_4O_3(PO_4)_3) = 1180(10)$ K has been determined.

$$VO_2 + VPO_4 + (VO)_2P_2O_7 \rightarrow V_4O_3(PO_4)_3 \quad (1)$$

To grow crystals of $V_4O_3(PO_4)_3$ suitable for X-ray single crystal investigation, a few milligrams of $PtCl_2$ as mineralizer are nessesary to allow vapor phase assisted reaction of the starting materials and improved recrystallization of the oxide phosphate. Again the starting materials were placed in a corundum crucible. The best crystals were achieved when the crucible was closed with gold foil. This "subampule" and 30 mg of $PtCl_2$ (as the source for chlorine as mineralizer) were sealed in an evacuated silica ampule and heated isothermally at 1073 K. After 5 days the tube was quenched and opened. Within the crucible single phase $V_4O_3(PO_4)_3$ (according to Guinier photographs) was obtained as black microcrystalline powder containing crystals with edge lengths up to 0.2 mm (Figure 2).

Equilibrium Experiments. Equilibrium experiments in the ternary system $(VO)_2P_2O_7/VPO_4/VO_2$ were carried out (sealed silica tubes, $T = 1073$ K, $t = 14$ d) by direct solid-state reaction. In some cases small amounts of iodine or $PtCl_2$ were used as mineralizer. To prevent reactions of the starting materials with the wall, corundum crucibles were used as reaction containers within the silica ampules. Details of the experiments are given in Table 2.

Substitution Experiments. Experiments aiming at substitution of vanadium(III) in $V_4O_3(PO_4)_3$ by other cations (M = Al, Ti, Cr, Fe, Rh, In) were carried out in a way similar to the equilibrium experiments described above (1073 K, pressed tablet, 20 mg of iodine as mineralizer, 7 days). Details on the experiments and their results are given in Table 3. While the experiment based on eq 1 led to pillars of intergrown crystals of $V_4O_3(PO_4)_3$ (Figure 2a), another one, aiming at substitution of V^{3+} by Al^{3+} with $AlPO_4$ as starting material, led to some rather isometric black crystals of the oxide phosphate with diameters up to 0.25 mm (Figure 2b). According to energy-dispersive X-ray (EDX) analysis, no aluminum was contained in these crystals.

Table 2. Equilibrium Experiments in the System $VO_2/(VO)_2P_2O_7/VPO_4$[a]

no.	starting material [mg]		mineralizer [mg]		reaction products (according to Guinier photographs)
1	VPO_4	142.2	*b*		$V_4O_3(PO_4)_3$, VO_2
	VPO_5	27.0			
	V_2O_5	29.8			
2	β-$VOPO_4$	280	iodine	50	$V_4O_3(PO_4)_3$, VPO_4
	VO_2	140			
	VPO_4	1270			
3	β-$VOPO_4$	602.0	iodine	50	$(VO)_2P_2O_7$, $V_4O_3(PO_4)_3$
	VO_2	124.0			
	VPO_4	892.0			
4	VO_2	45.1	$PtCl_2$	25	$V_4O_3(PO_4)_3$ and unknown weak diffraction lines
	$(VO)_2P_2O_7$	168.8			
5	VO_2	63.0	iodine	100	$V_4O_3(PO_4)_3$
	$(VO)_2P_2O_7$	234.0			
6	VO_2	40.0	*b*		$V_4O_3(PO_4)_3$
	$(VO)_2P_2O_7$	148.1			
7	VO_2	40.0	*b*		$(VO)_2P_2O_7$ and VO_2
	$(VO)_2P_2O_7$	148.1	1 atm air (RT)		

[a] Experimental conditions: 1073 K; $V = 24$ cm^3; heating time, 4−5 days. [b] Starting materials were pressed into a tablet. This was contained in a corundum crucible within the silica tube; no mineralizer was added.

X-ray Diffraction. An approximately spherical crystal (Figure 2b) was fixed on a silica glass fiber. Diffraction data were collected using a κ-CCD diffractometer (NONIUS). Structure determination and refinement, allowing for anisotropic displacement parameters and racemic twinning, proceeded in a straightforward manner. In the final refinement cycles a splitting of site V5 had to be introduced, indicating a mixed occupancy of this site by V^{3+} and V^{4+} ions (see Discussion). Details on the X-ray work are given in Table 5, and atomic coordinates for $V_4O_3(PO_4)_3$ are given in Table 6. Table 7 provides a summary of characteristic interatomic distances and angles. See Supporting Information for supplementary crystallographic information for $V_4O_3(PO_4)_3$.

For powder diffraction experiments a Guinier camera (Cu $K\alpha_1$ radiation, $\lambda = 1.54051$ Å, quartz monochromator, α-SiO_2 as internal standard) with image-plate foil has been used.[34] From such photographs taken at 293 K unit cell parameters for $V_4O_3(PO_4)_3$ have been determined as $a = 7.2596(8)$ Å, $b = 21.785(2)$ Å, and $c = 38.904(4)$ Å (program SOS).[35] Powder diffraction patterns for $V_4O_3(PO_4)_3$, $CrV_3O_3(PO_4)_3$, $FeV_3O_3(PO_4)_3$, and $V^{III}Ti^{IV}V^{IV}_2O_3(PO_4)_3$ are reproduced in Figure 3, and the corresponding lattice parameters are summarized in Table 4. Identification of the coexisting phases in the region $VO_2/(VO)_2P_2O_7/VPO_4$ of the V/P/O system by Guinier photographs was not an easy task because the characteristic reflections of $V_4O_3(PO_4)_3$ do coincide with some of the strongest reflections of $(VO)_2P_2O_7$ and VO_2. Furthermore, the existence of several vanadium oxides (Magnéli phases)[36] besides VO_2, with rather complicated X-ray powder patterns, made assignment of the diffraction patterns to individual phases very difficult.

(31) Schäfer, H. *Chemical Transport Reactions*; Academic Press, New York, 1964.
(32) Gruehn, R.; Glaum, R. *Angew. Chem., Int. Ed.* **2000**, *39*, 692−716.
(33) Johnson, J. W.; Johnston, D. C.; Jacobson, A. J.; Brody, J. F. *J. Am. Chem. Soc.* **1984**, 106, 8123−8128.
(34) Amemiya, Y.; Miyahara, J. *Nature* **1988**, *336*, 89−90.
(35) Soose, J. *Staatsexamensarbeit*; University of Giessen: 1985.
(36) Hyde, B. G.; Andersson, S. *Inorganic Crystal Structures*; John Wiley & Sons: Chichester, 1989.

Table 3. Experiments for Substitution of Vanadium(III) in $\square_2V_4O_3(PO_4)_3$

starting materials [mg]		mineralizer [mg]		*T* [K]	*t* [d]	reaction products (according to Guinier photographs)
$AlPO_4$	43.5	$PtCl_2$	25	1073	5	$\square_2V_4O_3(PO_4)_3$[a] and $AlPO_4$
VO_2	29.6					
$(VO)_2P_2O_7$	110.7					
TiP_2O_7	38.0	$PtCl_2$	29	1023	7	$\square_2V^{III}(Ti^{IV}V^{IV}_2)O_3(PO_4)_3$[b]
VPO_4	90.0					
VO_2	105.0					
$CrPO_4$	86.2	$PtCl_2$	25	1073	7	$\square_2CrV_3O_3(PO_4)_3$ (+ traces of β-$CrPO_4$)[45]
VO_2	48.5					
$(VO)_2P_2O_7$	180.6					
$FePO_4$	132.9	$PtCl_2$	20	1073	7	$\square_2FeV_3O_3(PO_4)_3$[c]
VO_2	71.0					
$(VO)_2P_2O_7$	263.8					
$InPO_4$	122.0	$PtCl_2$	25	1073	5	$(In_{1-x}V_x)PO_4$[d]
VO_2	48.0					
$(VO)_2P_2O_7$	179.0					
$RhPO_4$	95.0	$PtCl_2$	25	1073	5	$(VO)_2P_2O_7$, elemental Rh
VO_2	40.0					
$(VO)_2P_2O_7$	149.0					

[a] According to EDX analyses no aluminum is contained in the oxide phosphate. [b] We assume substitution of V^{4+} by Ti^{4+} due to oxidation of Ti^{3+} by V^{4+}. [c] The powder diagram of $\square_2FeV_3O_3(PO_4)_3$ is similar, however, different from that of $\square_2V_4O_3(PO_4)_3$ (Figure 3). [d] $X = 0.5(1)$ is estimated from comparison of the lattice parameters of $InPO_4$ [$a = 5.317(1)$, $b = 7.984(2)$, $c = 6.778(1)$ Å; re-determination by refs 46 and 47], VPO_4 [$a = 5.2316(5)$, $b = 7.7738(7)$, $c = 6.2847(5)$ Å][11] and $(In_{1-x}V_x)PO_4$ [$a = 5.2684(6)$, $b = 7.876(1)$, $c = 6.546(1)$ Å].

Table 4. Unit Cell Parameters of Mixed Oxide Phosphates $\square_2MV_3O_3(PO_4)_3$[a]

compound	*a* [Å]	*b* [Å]	*c* [Å]	no. reflections
$\square_2V_4O_3(PO_4)_3$	7.2622(7)	21.783(2)	38.902(4)	45
$\square_2CrV_3O_3(PO_4)_3$	7.246(1)	21.739(3)	38.785(6)	29
$\square_2V(TiV_2)O_3(PO_4)_3$	7.312(5)	21.93(1)	38.68(4)	19

[a] Determination from Guinier photographs (cf. Experimental Section).

Table 5. Crystallographic Data and Summary of Data Collection and Evaluation for $V^{III}V^{IV}_3O_3(PO_4)_3$

chemical formula	$V_{12}O_9(PO_4)_9$
formula weight	536.68 g/mol
crystal system	orthorhombic
space group	*F*2*dd* (No. 43)
a	7.2596(8) Å
b	21.786(2) Å
c	38.904(4) Å
V	6152(2) $Å^3$
Z	8
D_{calcd}	3.476 g/cm^3
radiation, wavelength, monochromator	Mo Kα ($\lambda = 0.71073$ Å), graphite
μ	4.10 mm^{-1}
color	black crystals, brown powder
diffractometer	κ-CCD (NONIUS) with area detector
crystal size	~0.23 mm
no. of measured reflections	85410
no. of independent reflections	6836
no. of observed reflections	83949
no. of reflections used in refinement	6836
no. of parameters	299
refinement on	F^2
R(*F*)/wR(F^2) (for all data)	0.044/0.066
weighting scheme	$w = 1/[\sigma^2(F_o^2) + (0.0284P)^2 + 14.4133P]$, where $P = (F_o^2 + 2F_c^2)/3$

Table 6. Atomic Coordinates and Isotropic Displacement Parameters for $V^{III}V^{IV}_3O_3(PO_4)_3$

atom	*x*	*y*	*z*	U_{eq}[a] [$Å^2$]
V1	0.10690(8)	−0.11404(2)	0.04761(1)	0.00582(7)
V2	0.09411(8)	−0.04280(2)	0.12572(1)	0.00606(7)
V3	0.79554(7)	0.05340(2)	0.11839(1)	0.00586(7)
V4	0.84342(7)	0.13391(2)	0.03251(1)	0.00612(7)
V5a	0.55280(17)	0.03691(5)	0.04277(3)	0.0054(2)[c]
V5b	0.53910(16)	0.03257(5)	0.03635(3)	0.0054(2)[c]
V6	0.30860(7)	−0.28658(2)	−0.04810(1)	0.00569(8)
P1	0.94090(17)	0	0	0.00518(17)
P2	0.20699(15)	−0.24859(3)	0.08201(2)	0.00533(14)
P3	0.95547(15)	0.16866(3)	0.16485(2)	0.00487(12)
*P*4	0.18811(14)	0.08673(2)	0.08189(2)	0.00526(13)
P5	0.45111(15)	−0.16786(3)	0.00027(1)	0.00495(13)
O1[b]	0.70079(37)	0.07560(9)	0.08257(5)	0.01112(37)
O2	0.18474(36)	−0.08432(8)	0.08286(5)	0.00961(37)
O3	0.46743(45)	0	0	0.01091(56)
O4	0.92468(32)	0.15804(9)	−0.00427(5)	0.00992(36)
O5	0.23603(32)	0.25739(8)	0.08469(4)	0.00942(40)
O11	0.05466(36)	−0.03876(8)	0.02348(5)	0.01231(43)
O12	0.81179(33)	0.04287(8)	0.02155(5)	0.00901(37)
O21	0.29309(35)	−0.29462(9)	0.05794(5)	0.01506(43)
O22	0.35167(31)	−0.20979(9)	0.09964(5)	0.01187(36)
O23	0.08470(34)	−0.28025(9)	0.10849(5)	0.01275(39)
O24	0.08316(33)	−0.20424(8)	0.05991(4)	0.00855(35)
O31	0.84225(36)	0.12886(8)	0.14148(4)	0.00966(37)
O32	0.84096(34)	0.20672(8)	0.18916(4)	0.00968(37)
O33	0.08854(32)	0.12668(8)	0.18563(4)	0.00842(34)
O34	0.07724(34)	0.21295(8)	0.14261(5)	0.00833(34)
O41	0.06254(35)	0.12266(9)	0.05849(5)	0.01405(42)
O42	0.31959(36)	0.04647(9)	0.06196(5)	0.01330(40)
O43	0.04400(34)	−0.12122(9)	0.14399(5)	0.01221(40)
O44	0.06414(32)	0.04336(8)	0.10424(4)	0.00811(36)
O51	0.31140(33)	−0.12772(9)	0.01796(5)	0.01158(38)
O52	0.35756(33)	−0.21497(9)	−0.02232(5)	0.01385(42)
O53	0.58147(36)	−0.19830(10)	0.02547(5)	0.01350(40)
O54	0.57087(35)	−0.12408(8)	−0.02334(4)	0.00895(36)

[a] U_{eq} = 1/3 trace of U_{ij} the tensor. [b] Numbering of O atoms: "Oxide oxygen" atoms are described by one digit, and they are linked to vanadium only. "Phosphate oxygen" atoms are numbered with two digits: *nm*, where *n* is the number of phosphorus and *m* refers to the oxygen atom with the *m*th longest distance *d*(P—O) to phosphorus atom *n*. [c] Refined isotropically with one parameter for V5a and V5b.

EDX Analysis. EDX analysis was carried out using a PV 9800 (Fa. EDAX). Scanning electron micrographs were taken using a DSM 940 (Fa. Zeiss).

Catalytic Testing. The catalytic properties of the mixed oxide phosphates $M^{III}V^{IV}_3O_3(PO_4)_3$ (M^{III}: V^{3+}, Cr^{3+}, Fe^{3+}) were evaluated in the selective gas-phase oxidation of *n*-C_4 (*n*-butane and 1-butene, 1 vol % in air each). The batches of the materials used for catalyst testing had been prepared without $PtCl_2$ as mineralizer to avoid any tampering of the catalytic performance by the presence of platinum. The mixed oxide phosphate powders were pressed to tablets in a tablet machine. The resulting tablets were chopped into granules (split) with a diameter distribution of 1.6−2.0 mm. The

Table 7. Interatomic Distances d(V−O) and d(P−O) in $V_4O_3(PO_4)_3$[a,b]

distance	*d* [Å]	distance	*d* [Å]	distance	*d* [Å]
V1−O2	1.618(2)	V2−O23^{i}	1.872(2)	V3−O1	1.628(2)
V1−O51	1.904(2)	V2−O43	1.886(2)	V3−O22^{x}	1.900(2)
V1−O11	1.927(2)	V2−O2	2.008(2)	V3−O31	1.904(2)
V1−O24	2.030(2)	V2−O5^{iv}	2.045(2)	V3−O34^{iv}	2.029(2)
V1−O33^{iv}	2.064(2)	V2−O44	2.066(2)	V3−O44	2.038(2)
V1−O4^{ii}	2.348(2)	V2−O34^{iv}	2.068(2)	V3−O5	2.500(2)
V4−O4	1.634(2)	V5a-O42	1.862(3)	V5b-O3	1.666(2)
V4−O21^{xi}	1.881(2)	V5a-O32^{v}	1.903(2)	V5b-O42	1.904(3)
V4−O41	1.901(2)	V5a-O3	1.949(2)	V5b-O32^{v}	1.944(2)
V4−O54^{xv}	2.022(3)	V5a-O54^{ii}	2.048(2)	V5b-O12^{vi}	2.070(2)
V4−O12	2.042(2)	V5a-O12^{vi}	2.057(3)	V5b-O54^{ii}	2.070(2)
V4−O1	2.546(2)	V5a-O1^{vi}	2.065(2)	V5b-O1^{vi}	2.343(2)
V6−O5^{ii}	1.646(2)	P1−O11^{ii}	1.493(2)	P2−O21	1.508(2)
V6−O52	1.888(2)	P1−O11	1.493(2)	P2−O22	1.513(2)
V6−O53^{xii}	1.898(3)	P1−O12^{ii}	1.567(2)	P2−O23	1.525(2)
V6−O24^{iii}	2.055(2)	P1−O12	1.567(2)	P2−O24	1.575(2)
V6−O33^{xiv}	2.074(2)				
V6−O4^{vii}	2.252(2)				
P3−O31	1.501(2)	P4−O41	1.508(2)	P5−O51	1.506(2)
P3−O32	1.508(2)	P4−O42	1.510(2)	P5−O52	1.512(2)
P3−O33	1.557(2)	P4−O43^{i}	1.520(2)	P5−O53	1.515(2)
P3−O34	1.569(2)	P4−O44	1.568(2)	P5−O54	1.584(2)

[a] Estimated standard deviations in parantheses. [b] Symmetry operators: (i) $x + 1/4, y + 1/4, -z + 1/4$; (ii) $x, -y, -z$; (iii) $x + 1/2, -y - 1/2, -z$; (iv) $x - 1/4, y - 1/4, -z + 1/4$; (v) $x + 3/4, y - 1/4, -z + 1/4$; (vi) $x + 1, y, z$; (vii) $x + 1/2, y - 1/2, z$; (viii) $x + 1, -y, -z$; (ix) $x - 1, y, z$; (x) $x - 3/4, y + 1/4, -z + 1/4$; (xi) $x - 1/2, y + 1/2, z$; (xii) $x - 1/2, -y - 1/2, -z$; (xiii) $x - 1/4, -y - 1/4, z + 1/4$; (xiv) $x + 1/4, -y - 1/4, z-1/4$; (xv) $x-1, -y, -z$.

catalyst materials were tested in an electrically heated reactor tube ($L = 100$ cm, inner diameter 13 mm) with an in situ gas chromatographic analysis of the products. The catalyst temperature was measured inside the reactor tube with a movable integrated thermocouple ($D = 3.17$ mm). The split was filled in the reactor tube with a height of 85 cm. In case of the *n*-butane oxidation (due to the low reactivity of *n*-butane) the undiluted split ($1.6 \leq D \leq 2.0$ mm) was tested. Because of the high reactivity of 1-butene the splitt had to be diluted with steatite balls ($1.5 \leq D \leq 2.5$ mm) in the 1-butene oxidation. Therewith the hot spot could be limited to a maximum of 20 K. The results for the selective oxidation of *n*-butane are given in Table 9 and for 1-butene in Table 10.[27]

Results and Discussion

Synthesis and Thermal Behavior. Microcrystalline $V_4O_3(PO_4)_3$ is black. The presence of the redox couple V^{3+}/V^{4+} gives rise to intense intervalence charge transfer, explaining the black color of larger crystals as well as the dark brown of $V_4O_3(PO_4)_3$ powder. The oxide phosphate melts at 1180 K.

We believe that isothermal heating of the starting materials close to the melting point of the desired product leads to improved recrystallization. Apparently, chlorine used as mineralizer (from the precursor $PtCl_2$) assists in a more rapid equilibration and crystallization of the oxide phosphates via heterogenous solid/gas reactions.

According to the equilibrium experiments at 1073 K, the phase triangles $VO_2/(VO)_2P_2O_7/V_4O_3(PO_4)_3$, $(VO)_2P_2O_7/V_4O_3(PO_4)_3/VPO_4$, and $VO_2/VPO_4/V_4O_3(PO_4)_3$ do exist (Figure 1). There is no evidence for a compound "$V_3P_2O_{11}$" mentioned in literature or any other vanadium(III,IV) oxide phosphate apart from $V_4O_3(PO_4)_3$.[23] Our experiments (Table 2, experiments 4−6) show also that at 1073 K two-phase mixtures $VO_2/(VO)_2P_2O_7$ decompose to a significant extent into $V_4O_3(PO_4)_3$ and oxygen (eq 2). From the experiment an equilibrium pressure $p(O_2)_{1073K} \sim 1.2$ atm is estimated. Consequently, thermal decomposition of the $VO_2/(VO)_2P_2O_7$ mixture is suppressed in ampules filled with air at room temperature [$p(O_2)_{1073K} \sim 2$ atm, Table 2, experiment 7]. It is worth noting that decomposition of $(VO)_2P_2O_7$ at 1073 K into VPO_4 leads to $p(O_2)_{1073K} \sim 10^{-12}$ atm[7] and that at the same temperature the oxygen equilibrium pressure over VO_2/V_8O_{15} reaches 10^{-8} atm.[29]

$$4VO_2 + 6(VO)_2P_2O_7 \rightarrow 4V_4O_3(PO_4)_3 + O_2(g) \qquad (2)$$

Crystal Structure. $V_4O_3(PO_4)_3$ belongs to the Lipscombite−Lazulite structure family, like β-V_2OPO_4, β-Fe_2OPO_4,[10] $Fe_{2-y}(OH)PO_4$ ($0 \leq y \leq 2/3$), $NiCrOPO_4$, $Ti_5O_4(PO_4)_4$,[24,25,37] and many others. The structure of β-Fe_2OPO_4,[10] the tetragonal aristotype of this family, is built up by phosphate groups and infinite chains of face-sharing [FeO_6] octahedra (Figure 4a,b). These chains are running parallel to the crystallographic *a*- and *b*-axis. Perpendicular chains are linked via common vertices ("oxide" oxygen with coordination number(O^{2-}) = 4) and [PO_4] tetrahedra. The octahedral voids are fully occupied by 50% divalent and 50% trivalent cations in β-V_2OPO_4, β-Fe_2OPO_4, and $NiCrOPO_4$, whereas in $Ti_5O_4(PO_4)_4$ only 5/8 of the octahedral voids are occupied by Ti^{4+} ions with the remaining 3/8 being empty. The crystal structure of $V_4O_3(PO_4)_3$, containing one V^{3+} and three V^{4+} per formula unit, shows an occupancy of 4/6 for the octahedral voids, corresponding to a formula $\square_2V_4O_3(PO_4)_3$. The occupancy sequence within each "chain" of octahedra is "...EOOEOO..." (E = empty, O = occupied). The unit cell of $\square_2V_4O_3(PO_4)_3$ ($Z = 24$) contains vanadium on six crystallographically independent sites [space group: *F*2*dd* (No. 43); Wyckoff position 16b]. This leads to three different types of [V_2O_9] dimers ([V1−V6], [V2−V3], and [V4−V5]; Figures 4 and 5). Two types of "chains" of octahedra can be distinguished. One is built up by dimers [V6−V1] and [V5−V4] intermitted by vacancies according to ...E, [V6−V1], E, [V5−V4], E, [V6−V1], E, [V5−V4], ... The second type contains only dimers [V3−V2] and vacancies corresponding to the sequence ...E, [V3−V2], E, [V3−V2], ... Sites V1, V3, V4, and V6 are occupied by V^{4+} ions. For these ions with highly distorted octahedral coordination one finds one rather short distance d(V−O) ∼ 1.63 Å, according to a vanadyl group $(V{=}O)^{2+}$, four equatorial oxygen atoms at 1.87 Å ≤ d(V−O) ≤ 2.07 Å, and a sixth oxygen ligand at 2.25 Å ≤ d(V−O) ≤ 2.55 Å (Figure 5). Site V2 shows distances of 1.86 Å ≤ d(V−O) ≤ 2.07 Å in agreement with a more regular octahedral coordination expected for V^{3+}. Electroneutrality requires for site V5 mixed occupancy by 50% V^{3+} and 50% V^{4+}, and indeed, the final structure refinement led to split positions V5a (V^{3+}) and V5b (V^{4+}). While V5a is just at the center of an octahedral void formed by O42, O32, O3, O12, O54, and O1, V5b is shifted toward O3, away from O1. Thus, the typical distances d(V−O) for V^{3+} and V^{4+} are realized within the structure (Figure 5). It is worth mentioning that no indication was found for a superstructure

(37) Dowty, E. *ATOMS − Program for Crystal Structure Visualization*; Shape Software: Kingsport, TN, 2004.

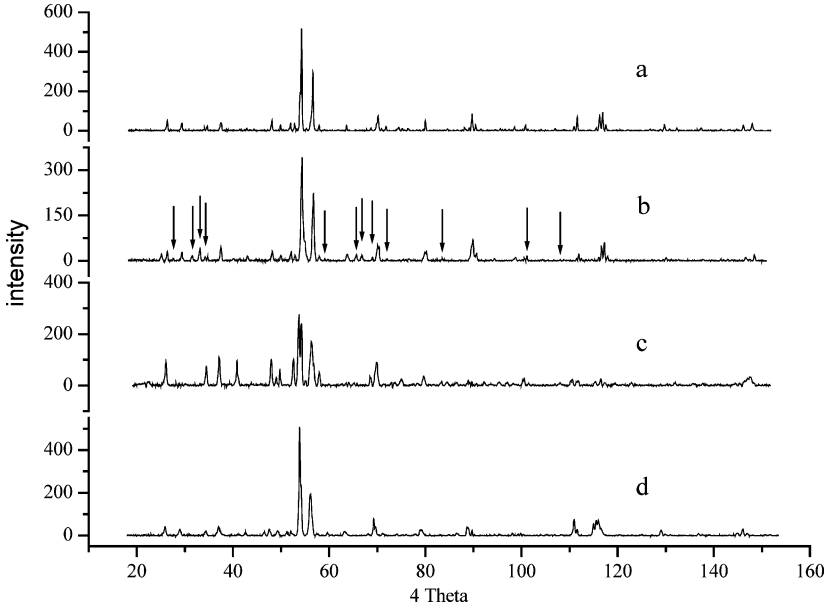

Figure 3. XRD pattern of $\square_2V_4O_3(PO_4)_3$ (a); $\square_2CrV_3O_3(PO_4)_3$ (b), arrows indicate β-$CrPO_4$; $\square_2FeV_3O_3(PO_4)_3$ (c); and $\square_2V(TiV_2)O_3(PO_4)_3$ (d).

Table 8. Survey of Ternary and Polynary Members of the Lipscombite/Lazulite Structure Family

compound	n^a	occupancy[b]	occupancy sequence[c]
$\square_3Ti_5O_4(PO_4)_4$[24,25]	4	5/8 (0.625)	EOOEOOEO...
$\square_{17}Ti_{31}O_{24}(PO_4)_{24}$[24,25]	3.87	31/48 (0.646)	unknown
$\square_2V_4O_3(PO_4)_3$	3.75	4/6 (0.667)	EOOEOO...
$\square MTi_2O_2(PO_4)_2$ (e.g., M = Ni^{2+})[43]	3.33	3/4 (0.750)	ETiMTiETiMTi...
$\square_2V_4[O(OH)_2](PO_4)_3$[38]	3.25	4/6 (0.667)	EOOEOO...
$\square_{0.77}V_{1.23}[(OH)_{0.69}(OH_2)_{0.31}](PO_4)\cdot 0.33H_2O$ [39]	3	1.23/2 (0.615)	unknown
$\square_1V(OH_2)(PO_4)$ (=$VPO_4\cdot H_2O$) [39]	3	1/2 (0.500)	EOEOEO...
$\square_0V_2O(PO_4)$ (= β-V_2OPO_4) [9)]	2.5	2/2 (1.000)	OOOOOO...

[a] *n* describes the average oxidation state of the metal cations M^{n+}. [b] Occupancy of the octahedral voids. [c] Distribution of the metal ions within the chains of face-sharing octahedral voids in the Lipscombite/Lazulite structure type: O, occupied; E, empty.

Table 9. Catalytic Oxidation of *n*-Butane to MA over Vanadium(IV) Oxide Phosphate Catalysts[a]

catalyst	T [K]	GHSV [h^{-1}]	$X_{n-\text{butane}}$ [%]	S_{MA} [%]	Y_{MA} [%]
$V^{3+}V^{4+}{}_3O_3(PO_4)_3$	693	800	15	40	6
$Cr^{3+}V^{4+}{}_3O_3(PO_4)_3$	703	800	40	15	6
$Fe^{3+}V^{4+}{}_3O_3(PO_4)_3$	703	800	15	15	2

[a] Reaction conditions: 1 vol % *n*-butane in air, no dilution of the catalyst split; GHSV (gas hourly space velocity) flow rate of air/butane mixture, $X_{n-\text{butane}}$ rate of transformation of *n*-butane, S_{MA} selectivity for msa, Y_{MA} yield of MA.

Table 10. Catalytic Oxidation of 1-Butene to MA over Vanadium(IV) Oxide Phosphate Catalysts[a]

catalyst	dilution[b]	T [K]	GHSV [h^{-1}]	$X_{n-\text{butane}}$ [%]	S_{MA} [%]	Y_{MA} [%]
$V^{3+}V^{4+}{}_3O_3(PO_4)_3$	1:8	693	1500	99.9	13	13
$Cr^{3+}V^{4+}{}_3O_3(PO_4)_3$	1:3	678	1200	99.9	17	17
$Fe^{3+}V^{4+}{}_3O_3(PO_4)_3$	1:1	693	1000	99.0	16	16

[a] Reaction conditions: 1 vol % 1-butene in air, split was diluted with inert steatite balls; GHSV (gas hourly space velocity) flow rate of air/butene mixture, $X_{1-\text{butene}}$ rate of transformation for 1-butene, S_{MA} selectivity for msa, Y_{MA} yield of MA. [b] Split was diluted with inert steatite balls ($1.5 \leq D \leq 2.5$ mm). A dilution of, e.g., 1:5 means that a 1 vol part of catalyst splitt ($1.6 \leq D \leq 2.0$ mm) was diluted with 5 vol parts of steatite balls.

that might allow ordering of the cations with two different oxidation states on site V5.

By occupying of face-sharing octahedral voids, dimers $V^{3+}-V^{4+}$ and $V^{4+}-V^{4+}$ are formed with distances d(V—V) around 3.06 Å. These give no reason to expect metal−metal bonding.

By their distances d(P—O) the phosphate groups can be classified into two groups. One group (P1, P3) exhibitis two short (1.49−1.51 Å) and two long (1.56−1.58 Å) distances, while for the second group (P2, P4, P5) three shorter distances (1.51−1.53 Å) and one rather long distance (1.58 Å) are observed. The longer distances result from a coordination of these oxygen atoms by three cations (two vanadium plus phosphorus), whereas oxygen connected to phosphorus at a rather short distance is bound only to one vanadium (Table 7). The five independent "oxidic" O^{2-} ions (in contrast to oxygen atoms in phosphate groups) in $\square_2V_4O_3(PO_4)_3$ are coordinated by three vanadium atoms. In the structure of the aristotype (e.g., β-$Fe_2O(PO_4)_2$,[10] β-$V_2O(PO_4)_2$[9]) the oxide ions are fourfold coordinated, due to the complete occupation of all octahedral voids by cations M^{2+} and M^{3+}.

Comparison to Other Members of the Lazulite/Lipscombite Structure Family. $\square_2V_4O_3(PO_4)_3$ and β-V_2OPO_4 are not the only representatives of this structure type within the family of the vanadium phosphates. The structure of hydrothermally synthesized $\square_2V_4O(OH)_2(PO_4)_3$[38] (closely related to $Fe_4(OH)_3(PO_4)_3$[38]) is very similar to that of $\square_2V_4O_3(PO_4)_3$. However, the presence of OH-groups (instead of O^{2-}) leads to a higher amount of V^{3+} with an average oxidation state +3.25 for vanadium in contrast to +3.75 in $\square_2V_4O_3(PO_4)_3$. Similarly, $\square V(OH_2)(PO_4)$ and $V_{1.23}[(OH)_{0.69}(OH_2)_{0.31}]$-

(38) Torardi, C. C. *J. Solid State Chem.* **1989**, *82*, 203−215.

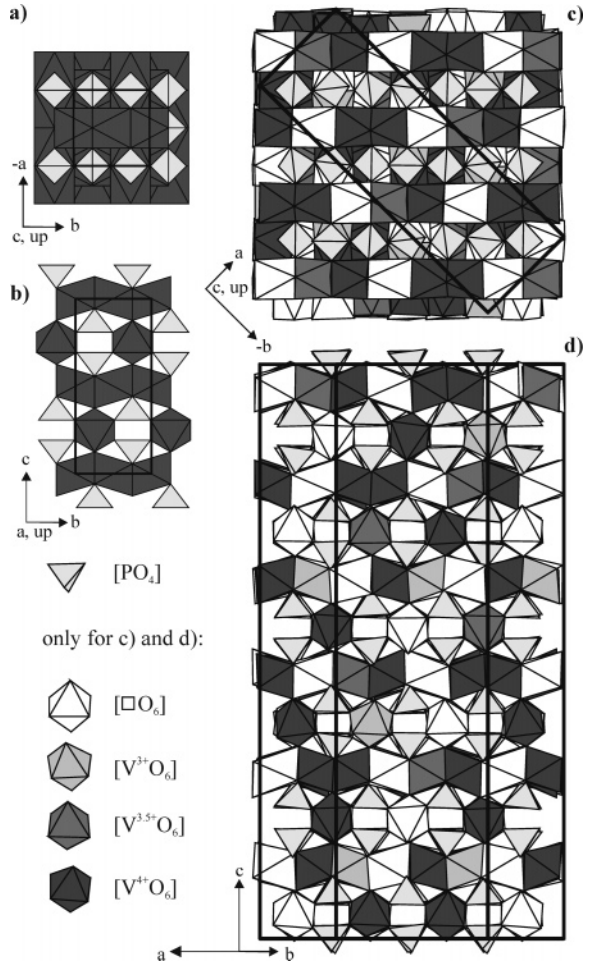

Figure 4. Structure relationship between β-$V_2O(PO_4)$ and $\square_2V_4O_3(PO_4)_3$. (a) Projection of the β-$V_2O(PO_4)$ structure onto (001) and (b) onto (100). (c) Projection of the $\square_2V_4O_3(PO_4)_3$ structure onto the (130) plane. Dark gray, $[V^{4+}O_6]$; gray, $[V^{3+}O_6]$; medium gray, $[V^{3+}/V^{4+}O_6]$; light gray, $[PO_4]$ white, $[oO_6]$. Visualizer software: ATOMS 6.2.[37]

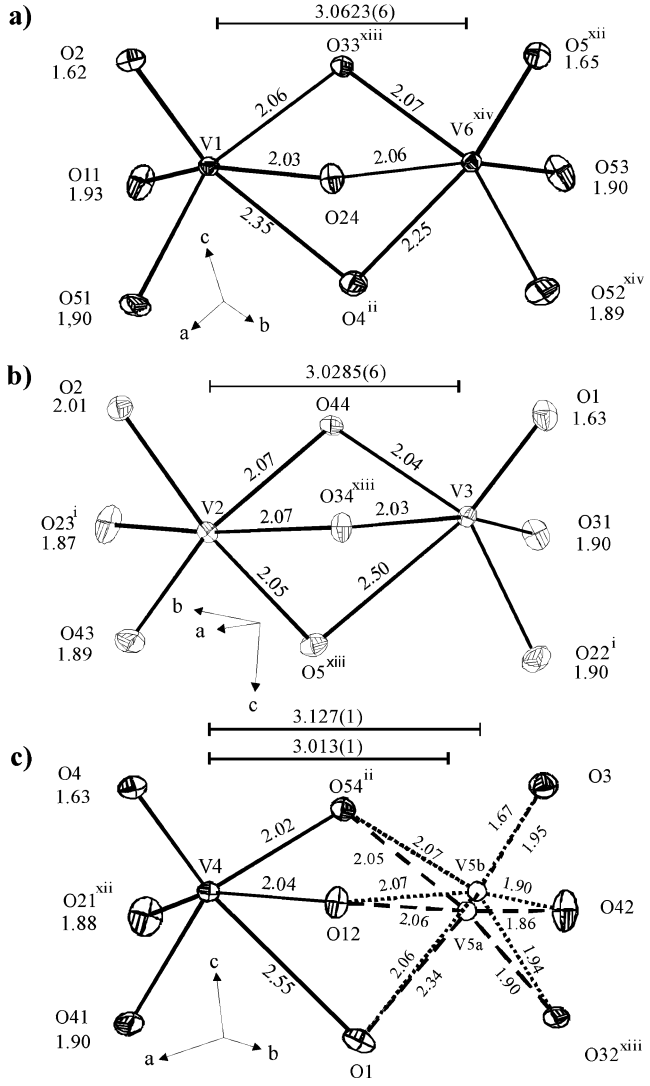

Figure 5. Dimers $[V_2O_9]$ in $V_4O_3(PO_4)_3$; distances in Å.

$(PO_4)\cdot 0.33H_2O$[39] containing purely V^{3+} belong to the Lazulite/Lipscombite structure family. While for $\square V(OH_2)(PO_4)$, described in literature as $VPO_4\cdot H_2O$,[39] occupied and empty octahedral voids are alternating, the structure refinement of $V_{1.23}[(OH)_{0.69}(OH_2)_{0.31}](PO_4)\cdot 0.33H_2O$ from powder data is not clear with respect to the cation distribution. In addition to the introduction of octahedral voids into the structure of β-$V_2O(PO_4)_2$ by oxidation of $V^{2+/3+}$ and/or substitution of O^{2-} by OH^- and OH_2 the structure type shows even more crystal chemical flexibility. Thus, titanium oxide phosphates $\square_3Ti_5O_4(PO_4)_4$, $Ti_{31}O_{24}(PO_4)_{24}$, and $Ti_4O_3(PO_4)_3$ with average oxidation states for titanium of +4.00, +3.87, and +3.75, respectively, have been characterized as members of the Lazulite/Lipscombite structure family,[24,25] with $Ti_4O_3(PO_4)_3$ being isotypic to $\square_2V_4O_3(PO_4)_3$.[26] Interestingly, there exists apparently no counter part to $\square_3Ti_5O_4(PO_4)_4$ with tetravalent vanadium (Figure 1). In the system Fe/P/O/H phases like $Fe_{4-x}Fe_{3x}(PO_4)_3(OH)_{3-3x}O_{3x}$ ($0.18 \leq x \leq 0.60$),[40] $Fe_{2-y}\square_y(PO_4)(OH)_{3-3y}(H_2O)_{3y-2}$ ($y = 2/3$ or 0.82),[41] $Fe_3(OH)_2(PO_4)_2$, and $Fe_{4.24}(PO_4)_3(OH)_{2.28}O_{0.72}$ have been crystallographically and chemically characterized. The latter hydroxy phosphates show catalytic activity in oxidative dehydrogenation of isobutyric acid to methacrylic acid.[42]

Even for mixed-metal oxide phosphates like $\square_3NiTi_2O_2(PO_4)_2$[43] and $NiCrO(PO_4)$[44] the Lipscombite/Lazulite structure type is realized. Table 8 gives a summary of various phosphates belonging to the Lipscombite/Lazulite structure family. Our experiments (Table 3) show that in $\square_2V_4O_3(PO_4)_3$ substitution of V^{3+} by Cr^{3+} or Fe^{3+} is possible. According to Guinier photographs (Figure 3) $\square_2CrV_3O_3(PO_4)_3$ is isotypic to the vanadium(III,IV) oxide phosphate. Unit cell parameters (Table 4) have been determined, giving a cell volume that is slightly smaller than that of the vanadium phosphate in agreement with expectation. "$\square_2FeV_3O_3(PO_4)_3$" has also been obtained in various experiments

(39) Vaughey, J. T.; Harrison, W. T. A.; Jacobson, A. J.; Goshorn, D. P.; Johnson, J. W. *Inorg. Chem.* **1994**, *33*, 2481−2487.
(40) Schmid-Beurmann, P. *J. Mater. Chem.* **2001**, *11*, 660−667.
(41) Song, Y.; Zavalij, P. Y.; Chernova, N. A.; Whittingham, M. S. *Chem. Mater.* **2005**, *17*, 1139−1147.
(42) Millet, J. M. *Catal. Rev. Sci. Eng.* **1998**, *40*, 1.
(43) Gravereau, P.; Chaminade, J. P.; Manoun, B.; Krimi, S.; El Jazouli, A. *Powder Diffr.* **1999**, *14*, 10−15.
(44) Ech Chahed, B.; Jeannot, F.; Malaman, B.; Gleitzer, C. *J. Solid State Chem.* **1988**, *74*, 47−59
(45) Attfield, J. P.; Batle, P. D.; Cheetham, A. K. *J. Solid State Chem.* **1985**, *57*, 357−361.
(46) Mooney, R. C. L. *Acta Crystallogr.* **1956**, *9*, 113−117.
(47) Görzel, H. Ph.D. Thesis, University of Giessen, 1998.

(Table 3). Its X-ray diffraction (XRD) pattern is similar to that of $\square_2V_4O_3(PO_4)_3$; however, differences in intensity and splitting of reflections (Figure 3c) indicate deviations from the orthorhombic structure of vanadium(III,IV) oxide phosphate. Work for further crystallographic characterization of "$\square_2FeV_3O_3(PO_4)_3$" is ongoing. Experiments aiming at a substitution of V^{3+} by Ti^{3+} (Table 3, experiment 2) led to a red-brown powder, with an XRD pattern (Figure 3d) almost identical to that of $\square_2V_4O_3(PO_4)_3$. Considering the redox behavior of $Ti^{3+/4+}$ and $V^{3+/4+}$ we believe that the charge distribution in the mixed titanium vanadium oxide phosphate corresponds to the formula $\square_2V^{III}(Ti^{IV}V^{IV}_2)O_3(PO_4)_3$. Further experiments did not provide any evidence for substitution of V^{3+} in $\square_2V_4O_3(PO_4)_3$ by Al^{3+}, In^{3+}, or Rh^{3+}.

The oxide phosphates $\square_2V_4O_3(PO_4)_3$, $\square_2CrV_3O_3(PO_4)_3$, and $\square_2FeV_3O_3(PO_4)_3$ studied in this investigation showed at least some activity for selective oxidation of *n*-butane and 1-butene to MA. The results for the selective oxidation of *n*-butane are summarized in Table 9 and for 1-butene are summarized in Table 10. In all tests CO_x were found as the only reaction products besides MA. The performance of the catalysts was stable during the testing period of 1 week. The catalyst materials showed no significant changes after the testing. At the optimum reaction temperatures between 660 and 730 K for the oxidation of *n*-butane lower activities (conversion rates $X_{n-\text{butane}}$; selectivities S_{MA}) were observed compared to the conventional vanadylpyrophosphate catalyst (e.g., $\square_2V_4O_3(PO_4)_3$ catalyst at 693 K: $X_{n-\text{butane}}$ 15%, S_{MA} 40%).

In the oxidation of 1-butene in all cases much higher conversion rates were observed than for the *n*-butane oxidation. The best novel mixed vanadium(IV) phosphate, $CrV_3O_3(PO_4)_3$, gave a MA yield of 17% (678 K: $X_{1-\text{butene}}$ 99%, S_{MA} 17%), with CO_x as the only byproduct. It is well-known that the oxidation of 1-butene at low conversion rates leads to ill-defined mixtures of oxygenates (e.g., CO_x, furane, butadiene, 2-butene, acetic acid, etc.). Because our main interest was the formation of MA, we did not investigate the oxidation of 1-butene under such conditions.

Conclusions

Systematic assessment of the ternary phase diagram V/P/O led to the discovery of the hitherto unknown, thermodynamically stable oxide phosphate $V_4O_3(PO_4)_3$. For its synthesis, accurate setting of the oxygen coexistence pressure is necessary. Its crystal structure belongs to the Lazulite/Lipscombite family. Inspired by this result, the search for polynary vanadium(IV) phosphates led to $\square_2CrV_3O_3(PO_4)_3$ and $\square_2FeV_3O_3(PO_4)_3$. The novel vanadium(IV) oxide phosphates show catalytic activity in the selective oxidation of *n*-butane and 1-butene to MA. Even though the catalytic properties of the novel phosphates do not yet reach the performance of vanadylpyrophosphate, our results are valuable extensions to the knowledge of catalysts for selective oxidations. The results show that addition of sesqui-oxides M_2O_3 and phosphates MPO_4 to vanadylpyrophosphate as promoting agents in many cases will lead to the formation of additional phases in the catalyst material, namely, of compounds belonging to the Lipscombite/Lazulite structure family. Even though the amount of these phases in the catalyst will hardly be detectable, they clearly influence its properties. Furthermore, our work demonstrates that certainly many more phosphates with properties similar or even superior to vanadylpyrophosphate can be found.

Acknowledgment. We thank Dr. Jörg Daniels and Norbert Wagner for the measurement at the κ-CCD and Prof. Dr. Johannes Beck for the friendly provision of the instrument.

Supporting Information Available: Crystallographic information for $V_4O_3(PO_4)_3$ (CIF). This material is available free of charge via the Internet at http://pubs.acs.org. This material has been deposited with FIZ (CSD-418195). Copies may be retrieved from Fachinformationszentrum Karlsruhe, Abt. IDNT, D-76344 Eggenstein-Leopoldshafen (e-mail: crysdata@fiz-karlsruhe.de).

CM071036U